

Article

Recovery of Rare Earth Elements from Mining Tailings: A Case Study for Generating Wealth from Waste

Luver Echeverry-Vargas ^{*} and Luz Marina Ocampo-Carmona 

Department of Materials and Minerals, Universidad Nacional de Colombia, Sede Medellín, Medellín 050034, Colombia; lmocampo@unal.edu.co

* Correspondence: ljecheverryv@unal.edu.co

Abstract: The growing demand for rare earth elements (REE) driven by their applications in modern technologies has caused the need to search for alternative sources of these elements as their extraction from traditional deposits is limited. A potential source of light rare earth elements (LREE) may be the monazite present in the mining waste generated in the Bagre-Nechí mining district in Colombia due to the processing of sands containing alluvial gold. Consequently, in this research, a systematic evaluation has been carried out for the extraction of *Ce*, *La*, and *Nd* from a leach liquor obtained from monazite present in alluvial gold mining tailings. The leaching process carried out with *HCl* indicated the recovery of approximately 90% of *La* and *Nd* and ~60% of *Ce*; the solvent extraction tests of these elements showed that increasing the contact time and pH of the leaching liquor positively affects the extraction of lanthanum, cerium, and neodymium, achieving extractions close to 100% with *D2EHPA* and to a lesser extent with *Cyanex 572*. McCabe–Thiele diagrams for extraction with *D2EHPA* indicated the requirement of three stages for the extraction of *Ce*, *La* and *Nd*.

Keywords: rare earth elements; solvent extraction; *D2EHPA*; *Cyanex 572*



Citation: Echeverry-Vargas, L.; Ocampo-Carmona, L.M. Recovery of Rare Earth Elements from Mining Tailings: A Case Study for Generating Wealth from Waste. *Minerals* **2022**, *12*, 948. <https://doi.org/10.3390/min12080948>

Academic Editor: Kenneth N. Han

Received: 24 May 2022

Accepted: 13 July 2022

Published: 28 July 2022

Publisher's Note: MDPI stays neutral with regard to jurisdictional claims in published maps and institutional affiliations.



Copyright: © 2022 by the authors. Licensee MDPI, Basel, Switzerland. This article is an open access article distributed under the terms and conditions of the Creative Commons Attribution (CC BY) license (<https://creativecommons.org/licenses/by/4.0/>).

1. Introduction

The extraction and processing of mineral resources cause environmental pollution and deterioration in some regions. After the completion of the geological processes and formation of the Earth's crust, all elements are in equilibrium. However, human intervention, even at the stage of geological prospecting, mobilizes the minerals concentrated in the Earth's crust. A commercial component and associated minerals in the development zone are activated, affecting the human habitat. After the beginning of development, the human habitat transforms into a domain of impact. Accumulated and stored industrial wastes are the most hazardous to the environment [1].

In the specific case of rare earth elements (REE), which are a group of chemical elements that include all the lanthanides (Ln), yttrium, and scandium, these elements are often divided into two categories: light rare earth elements (LREE), ranging from lanthanum to samarium, and heavy rare earth elements (HREE) ranging from europium to lutetium [2–4]. Due to their unique properties, REE are widely used in applications such as permanent magnets, energy storage systems, superconductors, electronics, and metal alloys. The importance of REE is growing every day due to their applications in modern technology and their consequent role in the fourth industrial revolution [5]. With the increasing global demand for REE in recent years, the traditional prospects of rare earth mining have started to be re-evaluated and new extraction possibilities have been considered [6–8]. Research carried out in the region of the Bagre-Nechí mining district in Colombia indicates the presence of monazite, with concentrations of rare earth oxides between 55 and 63% in the tailings of the mining operations [9,10].

Commercial rare earth concentrates have concentrations between 55 and 65% of rare earth oxides [11,12]. Although the REE content in tailings may be lower than in primary

sources, their processing can be justified if environmental benefits are considered, e.g., mine site remediation and land reclamation [13]; In addition, the identification of mining and industrial wastes with potential for utilization is currently a very relevant topic [1,4,14], as the development of innovative processes to extract elements of interest is not only a way to reduce the environmental impact of a company but also an opportunity to increase the useful life of the company after the depletion of reserves. Moreover, future REE supplies will likely rely on numerous unconventional resources other than classic ore deposits. Among these unconventional resources, low-grade deposits and tailings represent the next logical step for the mining industry, as shown by the decrease in minimum cut-off grades of all metals over time [15,16].

Monazite [(Ce, La, Nd, Th)PO₄] is a rare earth element (REE) phosphate [17] and is one of the most critical rare earth minerals in the world, serving as the main source of thorium and light rare earth elements (LREE) such as lanthanum, cerium, neodymium, and praseodymium [18]. The recovery of REE from monazite is not an easy task as REE are found forming a chain of polyhedra, in which each REE is linked to nine oxygen atoms forming the REEO₉ polyhedron, which in turn is linked to five tetrahedra of PO₄ [19,20] as shown in Figure 1. In the crystal structure of monazite, the REE–O and P–O bonds are covalent bonds. P–O bonds have a short bond length and a high chemical valence which greatly affects the lattice energy. Consequently, the structure becomes thermally and chemically stable [21]. Therefore, the presence of phosphate bonds in monazite ore hinders decomposition even at elevated temperatures, which affects overall REE recovery [22].

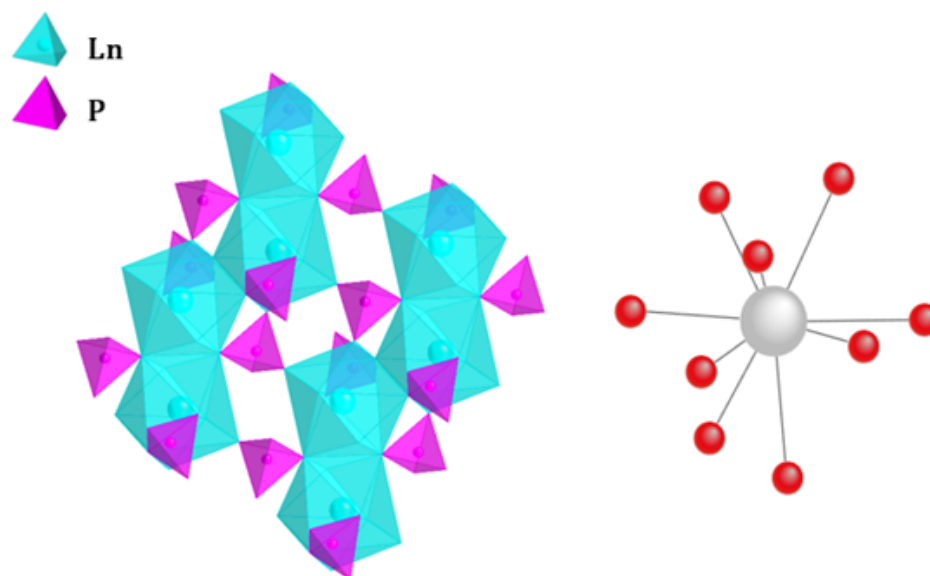


Figure 1. Schematic view of the crystal structure of monazite, $LnPO_4$. (Done by the authors).

REE ores such as monazite are generally processed in several stages (concentration, dephosphorization, leaching, and solvent extraction) [23]. These separation processes dramatically increase the percentage of REE phosphates in the final concentrate. The removal of REE from monazite concentrates generally involves decomposition of the phosphate structure; typically, the ore is decomposed with sodium hydroxide or potassium hydroxide to produce rare earth oxides. The resulting products are subsequently leached [24]; there are several hydrometallurgical treatments with inorganic acids to leach REE from their ores [25–27]. Different comparative studies have been published for the leaching of REE with different inorganic acids (HNO_3 , HCl , H_2SO_4), where the best leaching efficiencies were achieved with H_2SO_4 and HCl compared to HNO_3 [20,28].

Solvent extraction, or liquid-liquid extraction, is one of the most important separation processes in hydrometallurgy [29]. Among the various solvent extraction approaches, the use of organophosphorus extractants for liquid-liquid extraction of REE has been

highlighted [30–32]. Di-2-ethylhexyl phosphoric acid *D2EHPA* (Figure 2a) belongs to the class of organic phosphonic acids and is the most important investigated extractant in the separation of rare earth elements since the pioneering work of Miranda [33]. The main feature of *D2EHPA* is its ability to form a hydrogen bond between the extractant molecules, leading to the formation of dimeric structures [34], as can be seen in Figure 3a. In recent years, research and development of extractants for REE separation has focused on phosphonic acids with lower pKa value and sterically higher chain [35]. Accordingly, SOLVAY developed an extractant called *Cyanex*[®] 572, which is a mixture of phosphonic and phosphinic acids [35,36] (see Figure 2b), possibly like the *D2EHPA* extractant, *Cyanex* 572 also has the ability to form dimetric structures between phosphonic acid and phosphinic acid molecules (Figure 3b). The extensive use of organophosphorus extractants for the separation of rare-earth ions from aqueous solutions by solvent extraction is mainly due to their high sorption rate, chemical stability, and low aqueous solubility properties [29,37,38].

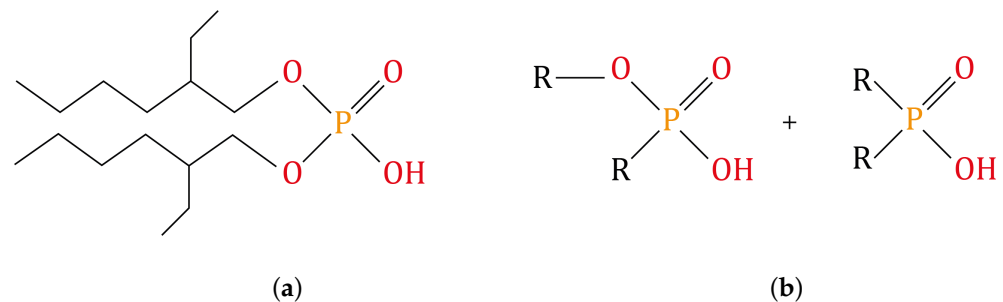


Figure 2. Molecular structure of the extractants used in this study; (a) *D2EHPA*, (b) *Cyanex* 572. (Done by the authors).

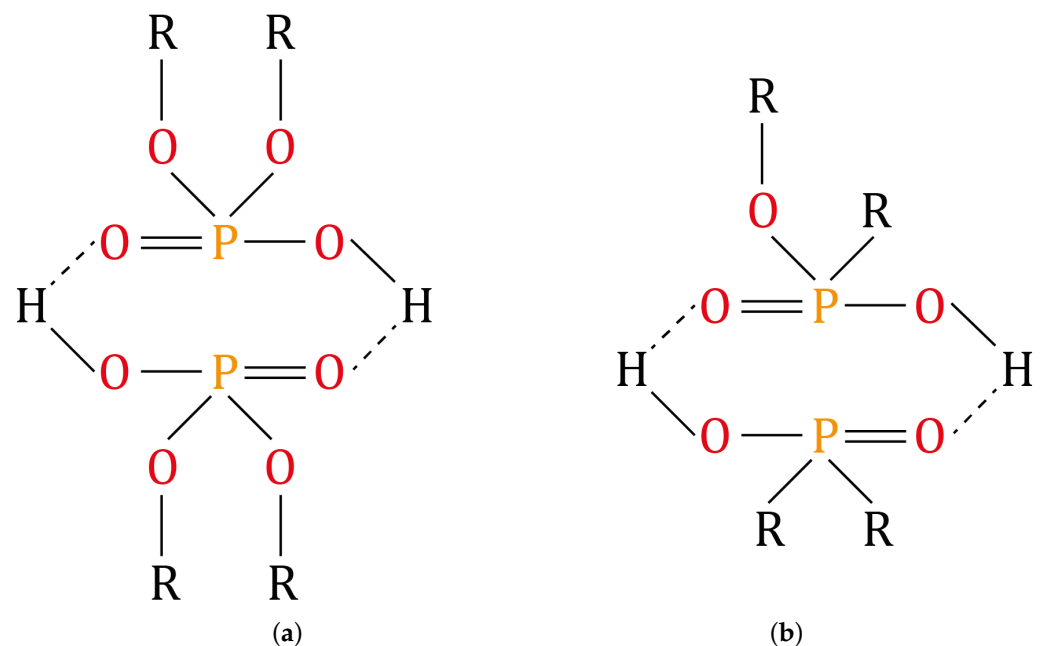


Figure 3. Dimetric structure of: (a) *D2EHPA*, (b) *Cyanex* 572. (Done by the authors).

Alluvial gold mining tailings from placer deposits in the Bagre-Nechí mining district region of Colombia are important sources of high economic value minerals such as monazite [9,10]. However, it can be observed that there are no detailed studies to determine the technical feasibility of extracting REE from these monazites, which is a highly relevant issue. Therefore, the purpose of this study was to determine the concentration, dephosphorization, and leaching conditions of monazite and to subsequently study the solvent extraction conditions of *Ce*, *La*, and *Nd*. To achieve this purpose, a monazite concentrate was first obtained from alluvial gold mining tailings from the Bagre-Nechí mining district

in Colombia by combining techniques including gravimetric, magnetic, and electrostatic separation; subsequently, phosphate removal conditions were evaluated with *KOH*. Next, the dephosphorized product was leached with *HCl*, and finally, the extraction of *Ce*, *La*, and *Nd* from the leaching liquor was studied using *D2EHPA* and *Cyanex 572* diluted in *n*-heptane as extractants. The dephosphorization conditions evaluated were treatment times and temperatures. In addition, an analysis of mineral species in the residue and monazite concentrate was performed; different parameters of the solvent extraction process were also evaluated systematically; the formation of organometallic phases was determined using log *D* vs. pH, slope analysis, and McCabe–Thiele diagrams. As *Ce*, *La*, and *Nd* are in the majority, the main focus of the studies was on these three elements.

2. Materials and Methods

2.1. Sample and Reagents

The ore sample used in this work was obtained from the waste tailings of the alluvial gold beneficiation process of the company Mineros Aluvial S.A.S BIC, Medellin, Colombia, whose operation is carried out in the Bagre-Nechi mining district (Antioquia, Colombia). Therefore, in this work, the initial sample corresponds to the product of gravimetric concentration using Jigs, which was subjected to free gold recovery processes; these waste sands were used as feed material in the monazite beneficiation process. A total of 1400 kg of sample was well mixed and homogenized for further concentration treatment. Sodium hydroxide (*NaOH*) was used as roasting reagents, Merck brand. Hydrochloric acid (PANREAC, Darmstadt, Germany 37%) was used as a leaching reagent; organic solutions for solvent extraction were obtained by diluting dis (2-ethylhexyl) phosphate (MERCK, Kenilworth, NJ, USA, 97%) and *Cyanex 572* (CYTEC INDUSTRIES BV, 100%) in *n*-heptane (MERCK, $\geq 99\%$). The pH required in the experimental solvent extraction tests was adjusted using dilute solutions of *NaOH* and *HCl*. Milli-Q water of 18.0 M Ω cm at 25 °C was used in all experiments.

2.2. Analysis of Mineral Species

The characterization of the crystalline phases before and after the concentration process was performed by X-ray diffraction (XRD) on a Panalytical X-Pert PRO MPD (Malvern PANalytical, Malvern, UK) in a 2θ interval between 3° and 70°, with a step of 0.02° and an accumulation time of 56 s; a copper anode with $K\alpha = 1.5406 \text{ \AA}$ was used. Characteristic diffraction peaks were identified from the COD (Crystallography Open Database). The constituent elements of the samples before and after the concentration process were analyzed in an ICP-OES (Inductively Couple Plasma-Optical Emission Spectrometer) model Optima 8300 from PerkinElmer, Waltham, MA, USA. Textural observations and elemental distribution maps of the monazite concentrate were obtained with a JEOL JSM 7100, JEOL, Tokyo, Japan, scanning electron microscope (SEM) with an imaging voltage of 15 keV. The elemental distribution maps of the characteristic low energy lines of each element were then extracted. Prior to SEM analysis, the surfaces of the ore specimens were coated with a thin layer of gold by sputtering.

2.3. Obtaining Monazite Concentrate

REE-containing minerals such as monazite have a relatively high specific gravity (between 4.9 and 5.5), which means that they can be initially separated from the gangue using gravimetric separation techniques; this primary separation can eliminate up to 90% of the gangue minerals [22,25]. In this work, 1400 kg of minerals were processed by gravimetric separation using a Wilfley laboratory concentrating table to separate the light gangue minerals (quartz, anorthite, cordierite, and greenalite) from the heavy ones (monazite, zircon, ilmenite, and magnetite); the concentrating table was operated at a dry feed rate of 0.8 kg/min and a water flow rate of 4.0 L/min. The oscillation speed was set at 300 oscillations/min and the platform angle at 10°. The first outlet at the front of the Wilfley table was considered as the concentrate, the second as media and the other

outlets were combined into a single tail. Separation on the concentrator table removed 34.1% of light minerals; after the gravimetric separation process, the heavy mineral fraction was subjected to a low-intensity magnetic separation process with an MIH (13) 111-5 CARPCO roller magnetic separator at 0.2T to recover monazite, zircon, and ilmenite. In this stage, 77.6% of the mineral was recovered; the non-magnetic product was taken to an electrostatic separation stage in a CARPCO HT (15, 25, 36) 111-15 reference equipment at 30.0 Kv to recover zircon and monazite, 72.6% of non-conductive minerals were recovered; in this stage, the separation of the different minerals is performed according to their conductivity [39]. To separate monazite from zircon, the non-conducting fraction was subjected to high-intensity magnetic separation at 1.5 T as rare earth elements generally have a series of electrons occupying the 4f subshell, and these electrons have magnetic moments that do not cancel, resulting in a material with some degree of magnetism [23], the magnetic fraction obtained was 2.3% corresponding to the monazite concentrate. A schematic diagram of the monazite concentration process is presented in Figure 4.

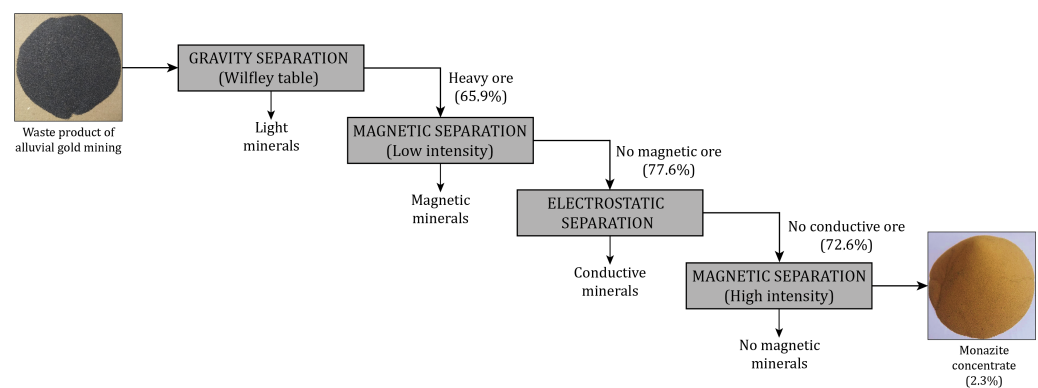


Figure 4. Flowsheet for concentrating monazite from alluvial gold mining residue. (Done by the authors).

2.4. Dephosphorization of the Monazite Concentrate

The obtained monazite concentrate was mixed with KOH as a baking reagent in a ratio (1:1) in a platinum crucible, according to reports in previous works [20,40]. These experiments were carried out at temperatures of 250, 300, 400, and 500 °C for 60, 90, and 120 min in an electric muffle. Each roasting product was rinsed with 250 mL of distilled water for 60 min with constant agitation to remove phosphate ions, then, the solution was filtered, and the residue was dried in an electric furnace. The dephosphorization products were characterized by ICP-OES (to quantify the main constituent elements) and X-ray diffraction to identify the different phases in which the rare earth elements are found. The percent phosphate removal from monazite was calculated using Equation (1) [20], where Pr indicates the percent phosphate removal, $W_f PO_4^{3-}$ indicates the phosphate present in a solution after water rinsing of the roasted monazite and $W_i PO_4^{3-}$ represents the phosphate present in the original monazite sample. Figure 5 shows the procedure followed for the removal of phosphate from the monazite concentrate.

$$Pr = \frac{W_f PO_4^{3-}}{W_i PO_4^{3-}} * 100 \quad (1)$$

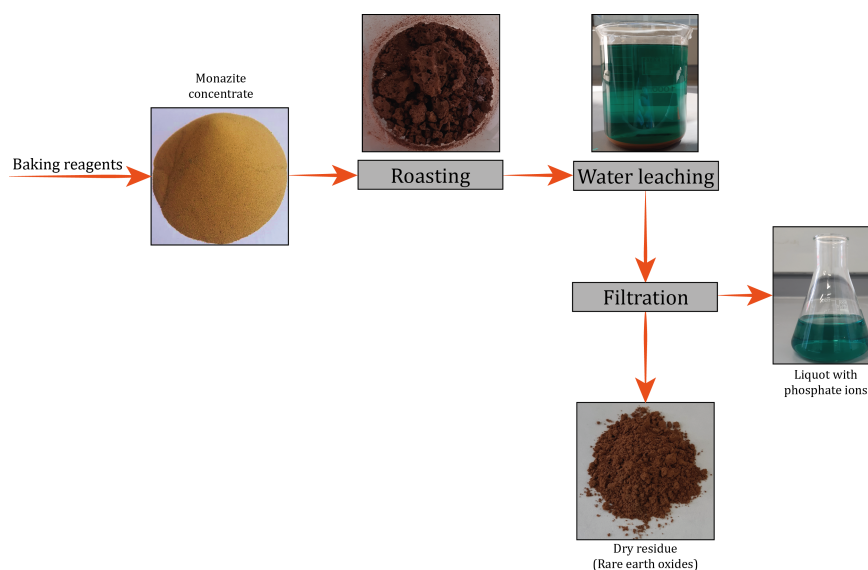


Figure 5. Flowsheet for the separation of phosphate from monazite concentrate via treatment with KOH . (Done by the authors).

2.5. Leaching of the Dephosphorized Product

The choice of acid during leaching depends on the subsequent separation process; H_2SO_4 is often chosen to facilitate separation by precipitation, whereas HCl is used for separation by solvent extraction. However, HNO_3 is generally avoided due to NO_x evolution and production of nitrated wastewater [20]. In this research, the monazite concentrate dephosphorized in the previous stage was leached with 6.0 M hydrochloric acid (HCl) at a temperature of 80 °C for a treatment time of 120 min, the leaching process was carried out in a three-hole Pyrex reactor equipped with a reflux condenser, the agitation was kept constant using a mechanical stirrer (300 rpm), and the pulp density was kept constant at 25 g/L. HCl concentration and temperature were previously determined in optimization experiments to provide satisfactory REE extraction [41]. The contents of lanthanum, cerium, and neodymium present in the leach solution were analyzed using a PerkinElmer Optima 8300 model ICP-OES. The extraction efficiency of lanthanides was evaluated by calculating the extraction (in %) using Equation (2). Where, C_E : lanthanide concentration in $mg L^{-1}$ at the evaluated condition; V_0 : volume of leaching solution, $V_0 = 0.3 L$ in all conducted experiments; m : mass of the initial dephosphorized rare earth concentrate, $m = 7500 mg$; $w\%$: mass fraction of lanthanides into the dephosphorized rare earth concentrate.

$$Extraction\ Efficiency\ (\%) = \frac{C_E * V_0}{m * w\%} * 100 \quad (2)$$

2.6. Solvent Extraction (SX)

Today a large number of extractants are available for use in hydrometallurgy, with more than 40 reagents available, of which approximately twelve are in everyday use; a detailed list of these reagents can be found in the work of Flett [29]. Solvent extraction of individual REE is a complex task due to the fact that these elements have similar physical and chemical properties; many extractable ions are in solutions, so a considerable number of separation steps are usually needed to produce a purified individual lanthanide element [42]. In this work, two extractants ($D2EHPA$ and $Cyanex\ 572$) were used to study the solvent extraction process of the lanthanide elements (Ce , La , and Nd) dissolved in the leach liquor. The organic phase was 10% v/v extractant in n -heptane; The effect of extraction time, equilibrium pH, and O/A ratio was investigated. For this, equal volumes of 25 mL of the aqueous and organic phases were mixed using a magnetic stirrer for 120 min at room temperature (25 °C). The organic and aqueous phases were then separated using a

separatory funnel; after phase separation, the metal concentrations in the aqueous phase were analyzed by ICP-OES. During the SX experiments, the concentrations of metals in the various organic phases were determined by mass balance. The distribution coefficient (D), extraction efficiency (%E), and separation factor (SF) were calculated as shown in Equations (3)–(5).

$$D = \frac{[C]_t - [C]_a}{[C]_a} \quad (3)$$

$$\%E = \frac{100 * D}{D + (V_{aq}/V_{org})} \quad (4)$$

$$SF = \frac{D_1}{D_2} \quad (5)$$

where $[C]_t$ is the initial metal concentration in the aqueous phase before extraction, $[C]_a$ is the metal concentration in the aqueous phase after extraction, V_{aq} is the volume of the aqueous solution and V_{org} is the volume of the organic solution. D_1 and D_2 denote the distribution ratios of two individual lanthanide metal ions.

3. Results and Discussion

3.1. Alluvial Mining Waste Analysis

As shown in Figure 6, the particle size analysis of the waste from alluvial gold mining indicates that the majority of the ore (40.6%) has a particle size between -60 and $+100$ mesh.

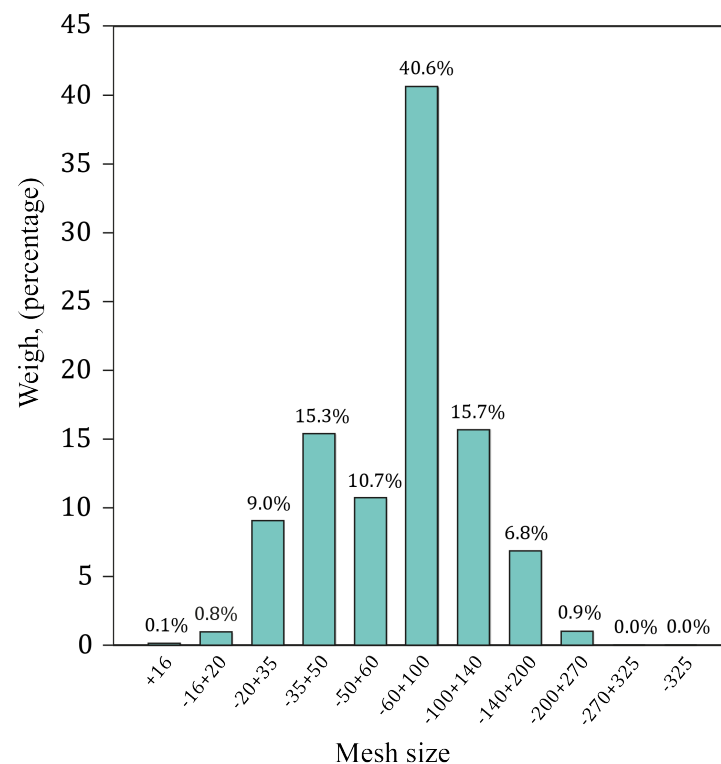


Figure 6. Grain size distribution of alluvial gold mining residue.

The main constituent minerals of the waste, determined by XRD analysis (Figure 7) indicate that monazite is the main REE-bearing mineral, ilmenite of titanium, and magnetite of iron oxides; in addition to zircon and quartz, confirming the observations of Lamus and Kerguelen [9,10]. Additionally, silicates such as anorthite, cordierite, and greenalite were identified. Table 1 shows the chemical composition of the waste, which reveals that the main constituents are iron and silica.

To recover the minerals of interest selectively in the beneficiation process, it is very important to understand and utilize the physical properties of the constituent minerals of the feed to the process. Specific gravity, magnetic susceptibility, and electrostatic susceptibility are the most representative differences in the physical properties of monazite, zircon, ilmenite, magnetite, and quartz, which can aid in their separation [3,22,43].

Quartz, which has a relatively low density (2.7 g/cm^3), can be separated relatively easily from ilmenite (4.7 g/cm^3), zircon (4.7 g/cm^3), and monazite ($4.9\text{--}5.5 \text{ g/cm}^3$), which have a high density, by gravimetric separation. On the other hand, monazite, ilmenite, and magnetite, which are paramagnetic minerals, can be separated from zircon and quartz, which are diamagnetic minerals. It has been reported that ilmenite and monazite can be separated by controlling the magnetic intensity [5]. Furthermore, by electrostatic difference, monazite (non-conductive mineral) can be separated from ilmenite and magnetite, which are conductive minerals [44].

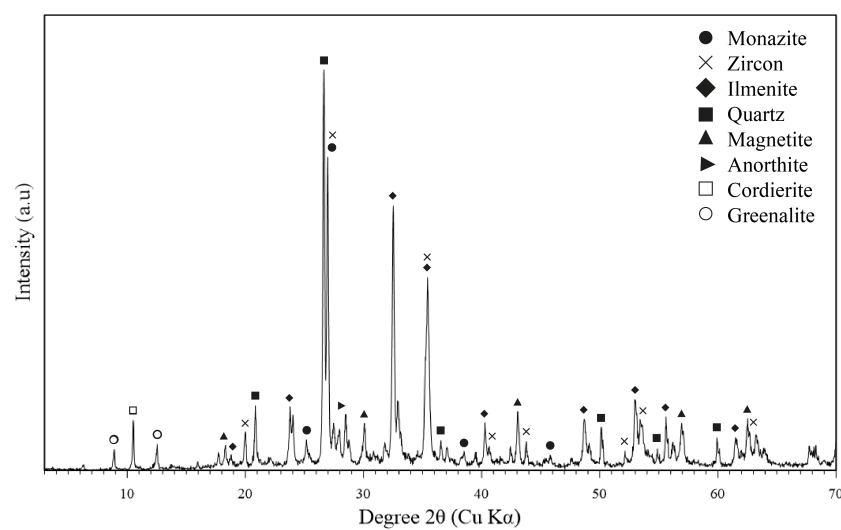


Figure 7. XRD diffractogram of the alluvial gold mining residue.

Table 1. Chemical composition by ICP-OES of the alluvial gold mining residue.

Components	Percentage, %(<i>w/w</i>)
Si	33.7
Fe	18.4
Ce	1.3
La	0.5
Nd	0.3
Pr	0.09
Zr	0.01
Y	0.07
Th	0.15
U	0.008
PO_4^{3-}	18.4
Others	Balance

3.2. Monazite Concentrate

The monazite concentrate obtained in this work presented particle size variation ranging from +16 to −325 mesh. The particle size analysis of the concentrate sample indicated that most of the monazite has a particle size between −140 and +200 mesh, as shown in Figure 8. Diffraction peaks of monazite, zircon, and magnetite were found in the XRD analysis, as can be seen in Figure 9.

Energy-dispersive X-ray spectroscopy (EDX) mapping was used to calculate the elemental composition of each particle in the monazite concentrate sample. As shown in

Figure 10, the most abundant elements are *P*, *Ce*, *La*, and *Nd*, associated with the monazite composition, while *Zr* and *Fe* are associated with zircon and magnetite, which are found in smaller proportions.

Chemical analysis (Table 2) of the monazite concentrate reveals that the sample contains 9.7% *La*, 21.3% *Ce*, 1.3% *Pr*, 8.7% *Nd*, and 3.5% *Th*. The phosphate content found in the form of PO_4^{3-} was 26.1%.

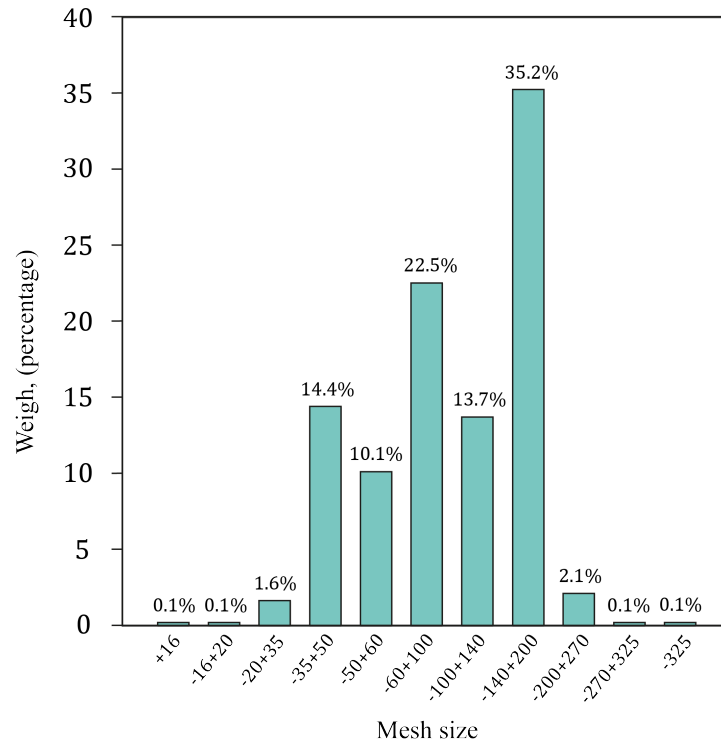


Figure 8. Grain size distribution of monazite concentrate.

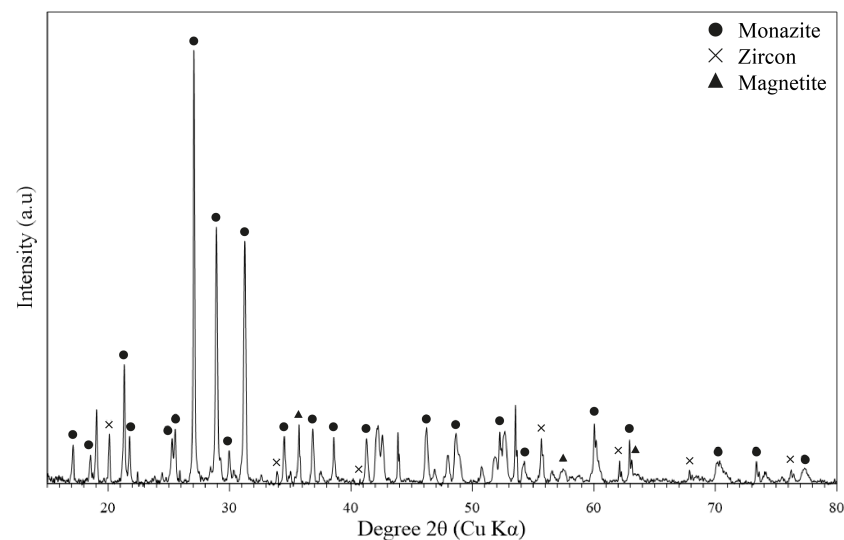
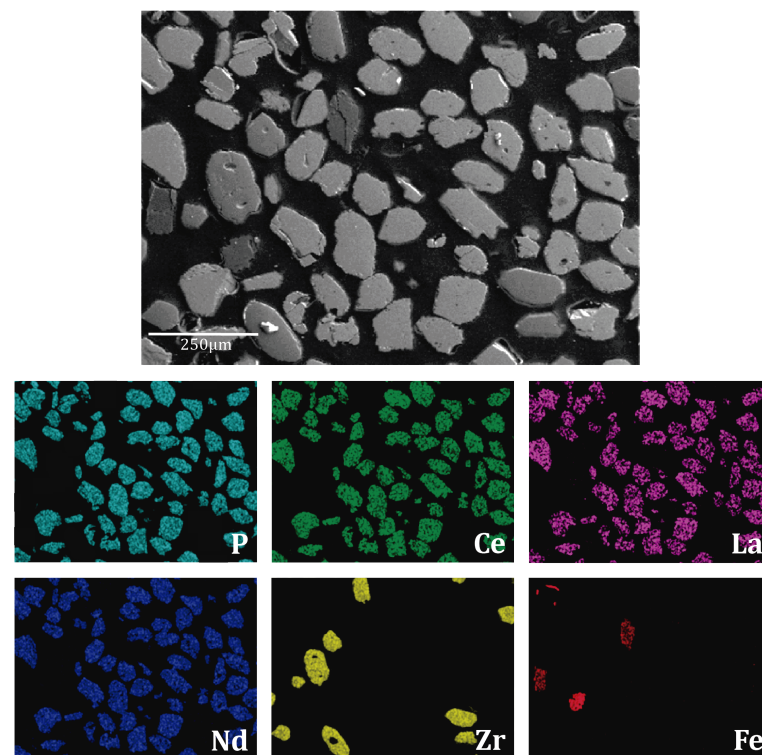


Figure 9. XRD diffractogram of the monazite concentrate.

Table 2. Chemical composition by ICP-OES of the monazite concentrate sample.

Components	Percentage, %(w/w)
Ce	21.3
La	9.7
Nd	8.7
Pr	1.3
Zr	0.5
Y	1.4
Th	3.5
U	0.3
PO_4^{3-}	26.1
Others	Balance

**Figure 10.** EDX mapping analysis of the monazite concentrate sample.

3.3. Dephosphorization of Monazite Concentrates

The phosphate removal efficiency is shown in Figure 11; it can be noted that the increase in temperature increases the phosphate removal efficiency at the times evaluated; in addition, with the increase of temperature from 250 to 500 °C and maintaining a treatment time of 60 min, phosphate removal increases from 83.3% to 86.0%. By increasing the treatment time to 90 min, the dephosphorization goes from 83.9% to 86.2% when the temperature is increased from 250 to 500 °C. It is possible to see that, by increasing the treatment time to 120 min, phosphate removal increases from 80.0% to 86.4% when the temperature goes from 250 to 500 °C. The chemical reaction that occurs when using *KOH* as roasting reagents is presented in Equation (6) [20].



The dephosphorization process of the monazite concentrate indicates that there is a greater removal of phosphate at a temperature of 500 °C; however, there are very similar phosphate removal percentages in the three times evaluated, which are around 86%. Figure 12 shows the diffraction patterns of the monazite concentrate after the roasting process with *KaOH* at 500 °C for 60, 90, and 120 min. A peak of $LaPO_4$ is found, indicating

that the dephosphorization process was not complete; the main REO diffraction peaks for the roasted mass show the presence of CeO_2 , La_2O_3 , Nd_2O_3 and ThO_2 . Table 3 shows the chemical composition of the dephosphorized product, with 5.7% phosphate as PO_4^{3-} , 33.1% cerium, 15.7% lanthanum, 16.2% neodymium, 2.0% praseodymium, 1.0% zirconium, 7.8% thorium, and 1.0% uranium.

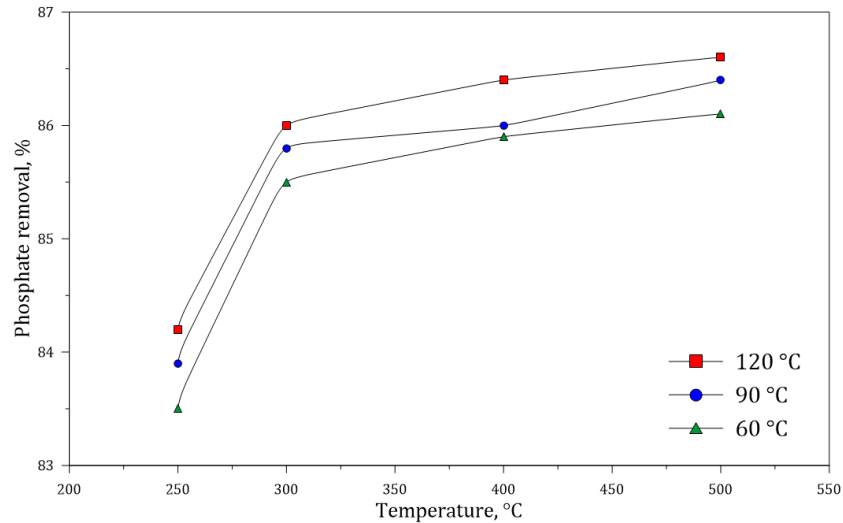


Figure 11. Effect of roasting temperature with KOH on the dephosphorization of monazite concentrate at times of 60, 90, and 120 min.

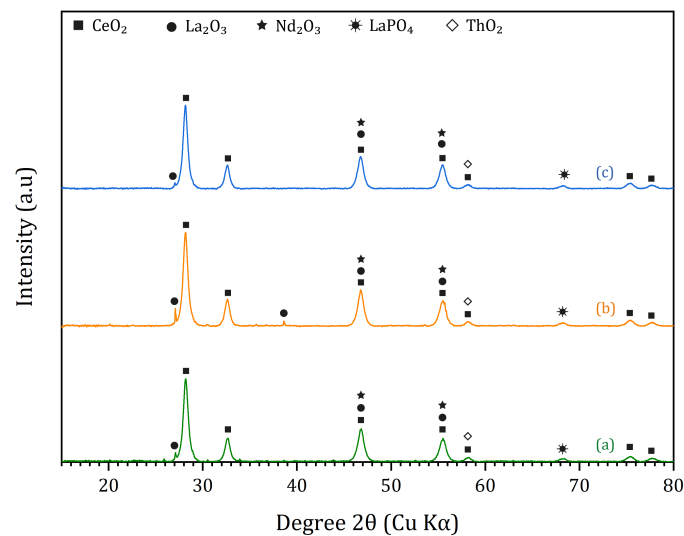


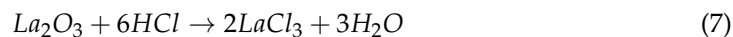
Figure 12. X-ray diffraction patterns of the monazite concentrate after the roasting process at 500 °C at times of (a) 60 min; (b) 90 min; (c) 120 min.

Table 3. Chemical composition by ICP-OES of the monazite concentrate after the roasting process at 500 °C, at time of 120 min.

Components	Percentage, % (w/w)
Ce	33.1
La	15.7
Nd	16.2
Pr	2.0
Zr	1.0
Y	2.2
Th	7.8
U	1.0
PO_4^{3-}	5.7
Others	Balance

3.4. Leaching Process

The leaching efficiency for *Ce*, *La*, and *Nd* are presented in Figure 13. 60.2 of Cerium was leached, while lanthanum presented a leaching efficiency of 92.8% and neodymium 94.3%. *La* and *Nd* oxides leached according to Equations (7) and (8) [45].



The lower extraction yield for cerium is not clear, but it is possibly associated with the fact that *Ce* is oxidized from its trivalent to a tetravalent state (Ce^{3+} to Ce^{4+}) during the roasting process and exists as CeO_2 [20] according to Equation (9).



In this case, CeO_2 is poorly soluble in *HCl*; a higher oxidation state in *Ce* favors the dissolution of *La* and *Nd* [46]. The results indicate that the oxidation capacity of CeO_2 improves with the increase of hydrogen ion concentration due to the high acid concentration. This leads to the formation of soluble compounds. The reaction involved during leaching of CeO_2 in *HCl* is presented in Equation (10) [47].

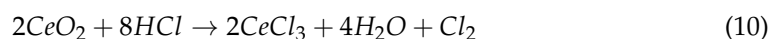


Table 4 shows the elemental analysis of the pregnant leaching liquor obtained under the conditions evaluated, the lixiviation efficiencies of *Ce*, *La*, and *Nd*, were calculated from Equation (2).

Table 4. Chemical analysis of pregnant leach liquor was obtained under the conditions evaluated.

Component	Units	Elemental Analysis		
		<i>Ce</i>	<i>La</i>	<i>Nd</i>
Feed solid	% (w/w)	23.3	10.7	10.5
Pregnant leach liquor	mg/L	3512.5	2477.0	2475.4
Pregnant leach liquor	mol/L	0.025	0.018	0.014
Leaching efficiency	%	60.2	92.8	94.3

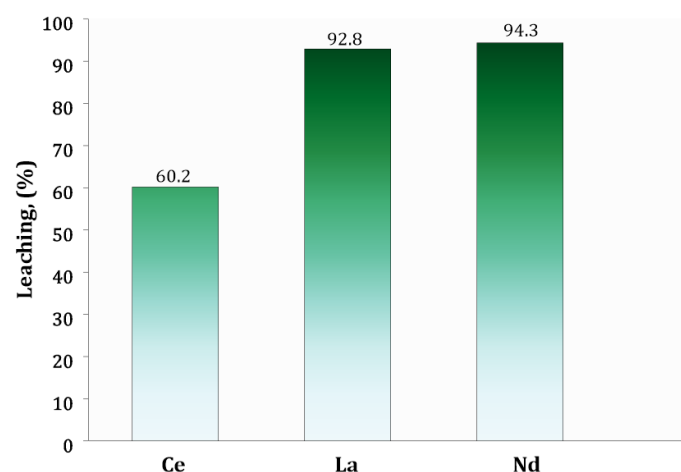


Figure 13. Leaching efficiency of *Ce*, *La*, and *Nd* in *HCl* 6.0 M.

3.5. Solvent Extraction

3.5.1. Effect of Contact Time

A series of experiments were carried out at different time intervals to observe the effect of contact time on the extraction of *La*, *Ce*, and *Nd*; the leaching liquor was mixed with 10% *D2EHPA* in n-heptane and 10% *Cyanex 572* in n-heptane, maintained an O/A

ratio of 1:1, at room temperature (25 °C). Considering previous experiments, the contact time of the mixture was varied from 5 to 120 min in the system with *D2EHPA* and from 5 to 720 min in the system with *Cyanex 572*; in Figure 14a it can be observed that when using *D2EHPA* the extraction of *La*, *Ce* and *Nd* increases with time, approximately 20.0% of *La*, 43.0% of *Ce* and 61.3% of *Nd* were extracted in 30 min at pH 0.5; it could also be observed that when using *Cyanex 572* the extractions of *La*, *Ce*, and *Nd* were approximately 5.6%, 12.5%, and 14.6%, respectively, in 360 min of contact at pH 0.5 (Figure 14b). Increasing the contact time in both systems had no significant effect on the extraction; therefore, a contact time of 30 min for *D2EHPA* and 360 min for *Cyanex 572* was considered optimal for all experiments performed.

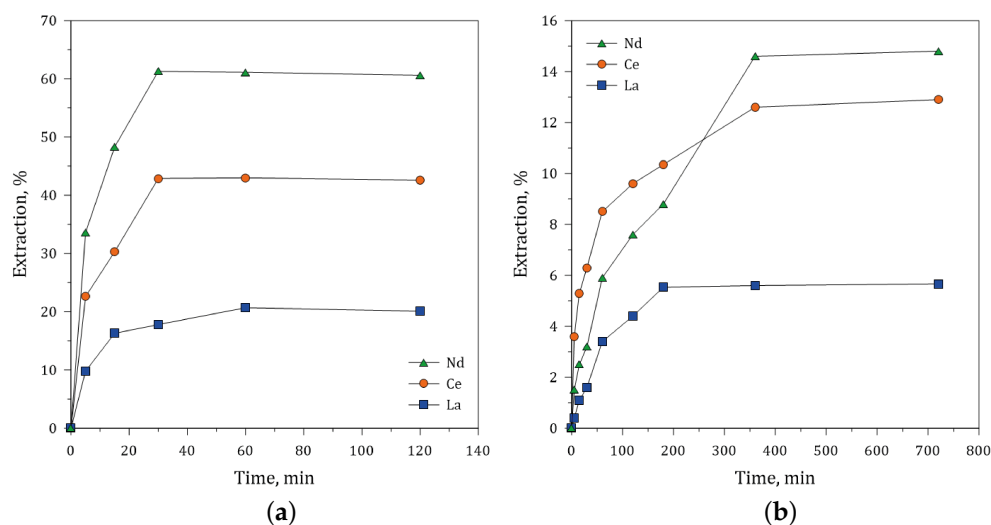


Figure 14. Effect of contact time on the extraction of *La*, *Ce* and *Nd* with: *D2EHPA* (a) and *Cyanex 572* (b).

3.5.2. Effect of pH

During extraction of metals using acidic extractants, H^+ ions are released, causing a decrease in pH, which subsequently lowers the extraction of metals. So, a series of experiments were carried out by varying the pH of the leaching liquor from 0.2 to 2.5, maintaining a contact time of 30 min for extraction with *D2EHPA* and 350 min for extraction with *Cyanex 572*; the required pH of the aqueous was adjusted using *NaOH* or *HCl* solution. The results indicate that the extraction of *La*, *Ce*, and *Nd* increases with pH with both extractants (see Figure 15a,b). The maximum extraction of *La*, *Ce* and *Nd* was 99.3%, 99.7% and 99.7% respectively with *D2EHPA* and 78.4% for *Ce*, 48.4% for *La* and 87.9% for *Nd*, respectively with *Cyanex 572*; these extractions are achieved at a pH of 1.5 for *D2EHPA* and 2.0 for *Cyanex 572*. A further increase in pH in both cases shows a minimal increase in the extraction of these elements.

Log *D* vs. pH plots were performed for the extraction with *D2EHPA* and *Cyanex 572* as can be seen in Figures 16 and 17; for the extraction with *D2EHPA*, straight lines with slopes 1.88, 1.98, and 1.79 were obtained for *Ce*, *La* and *Nd* respectively, which is indicating the release of 2 moles of H^+ per metal ion, similar behavior has been reported in other works [48,49]; in the case of extraction with *Cyanex 572* the slopes of the log *D* versus pH plots were 0.769 for *Ce* and 0.7596 for *La* and 0.9847 for *Nd*, respectively; indicating that the extraction of these elements followed a cation exchange mechanism, and a proton is related in the extraction reaction. The number of extractant molecules associated with the metal atom in the extracted species or the number of hydrogen ions released upon formation of the extracted species is not an integer in the cases under study; this situation arises because several different metal complexes are extracted simultaneously.

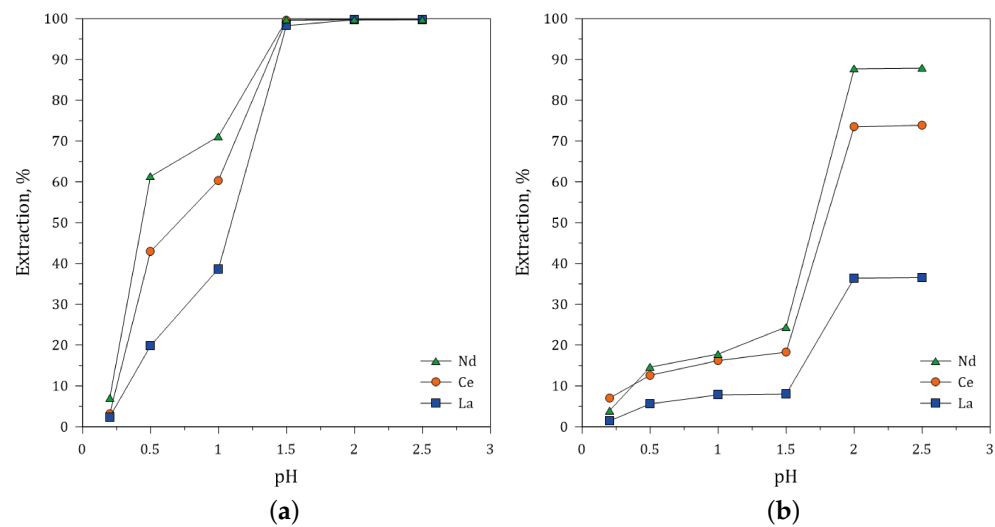
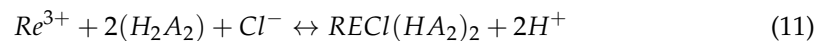


Figure 15. Effect of pH on the extraction of *La*, *Ce* and *Nd* in: *D2EHPA* (a) and *CY572* (b).

The extractants *D2EHPA* and *Cyanex 572* extract the metal from the aqueous solution by hydrogen ion exchange; these extractants produce dimers through hydrogen bonds, which can be represented by $(HA)_2$ or H_2A_2 for *D2EHPA* and H_2BC for *Cyanex 572* [20,50]. Therefore, based on the analysis of the slopes of the Log *D* vs. pH plots, the extraction reactions of trivalent rare earths (RE^{3+}) in a leach liquor in chloride medium with *D2EHPA* (HA) and *Cyanex 572* ($HB + HC$) in *n*-heptane can be expressed by Equations (11) and (12).



The equilibrium constants can be expressed as indicated below in Equations (13) and (14).

$$K_{D2EHPA} = \frac{[RECl(HA_2)_2][H^+]^2}{[RECl^{2+}][H_2A_2]^2} \quad (13)$$

$$K_{Cyanex\ 572} = \frac{[RECl_2HBC][H^+]}{[RECl_2^+][H_2BC]} \quad (14)$$

Replacing $[RECl(HA_2)_2]/[RECl^{2+}]$ and $[RECl_2HBC]/[RECl_2^+]$ by *D*; Equations (13) and (14) can be written as Equations (15) and (16).

$$K_{D2EHPA} = \frac{[D][H^+]^2}{[H_2A_2]^2} \quad (15)$$

$$K_{Cyanex\ 572} = \frac{[D][H^+]}{[H_2BC]} \quad (16)$$

Taking logarithms in Equations (15) and (16) and rearranging gives Equations (17) and (18).

$$\text{Log } D = \text{Log } K_{D2EHPA} + 2\text{Log } [H_2A_2]^2 + 2pH \quad (17)$$

$$\text{Log } D = \text{Log } K_{Cyanex\ 572} + [H_2BC] + pH \quad (18)$$

According to Equations (17) and (18), it can be said that *D* is a function of the pH and the concentration of the extracting agents. According to our speculation, considering the obtained results, the structure of the extracted species REH_2ClA_4 and $REHClBC$ is shown in Figure 18; however, more research is needed before drawing conclusions.

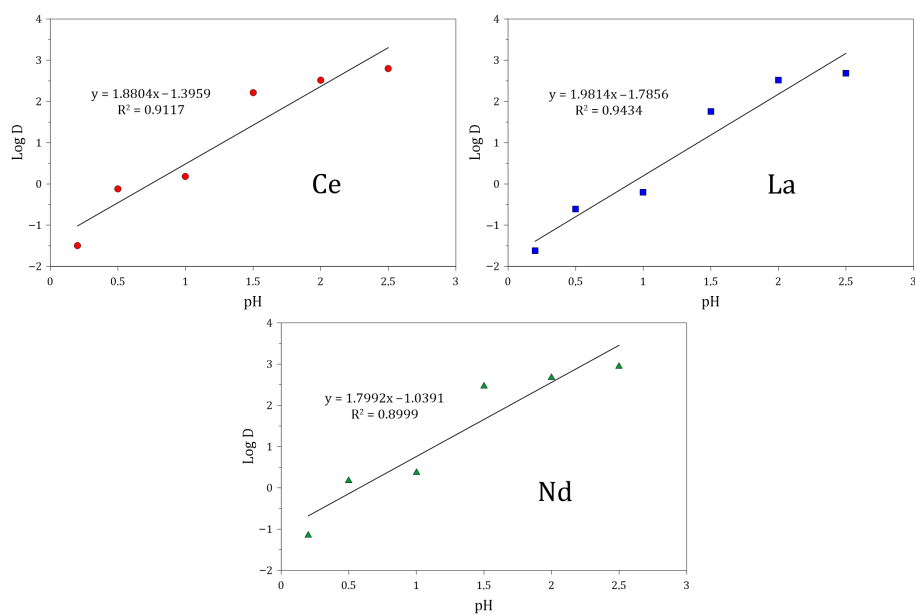


Figure 16. Log D vs. pH for the extraction of *Ce*, *La*, and *Nd* with D2EHPA.

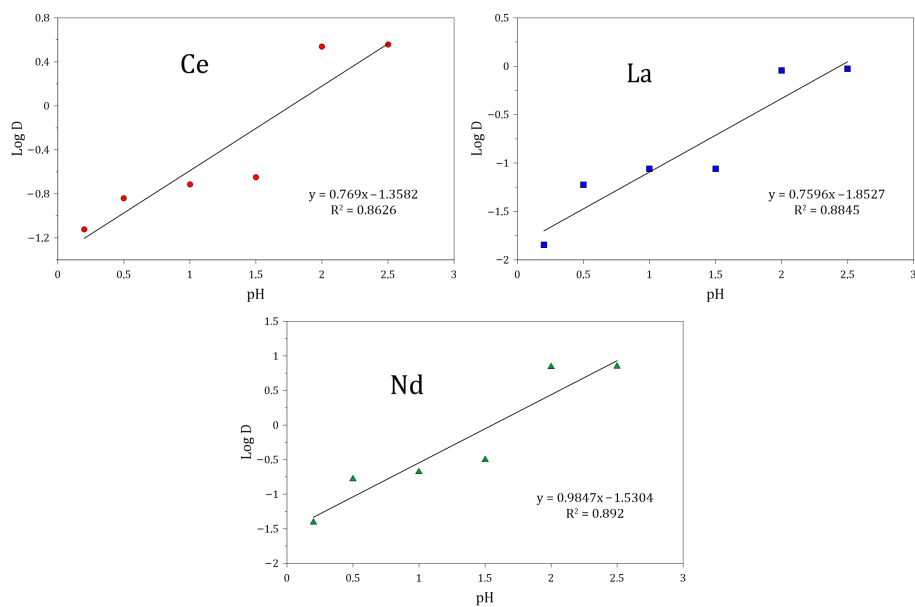


Figure 17. Log D vs. pH for the extraction of *Ce*, *La*, and *Nd* with Cyanex 572.

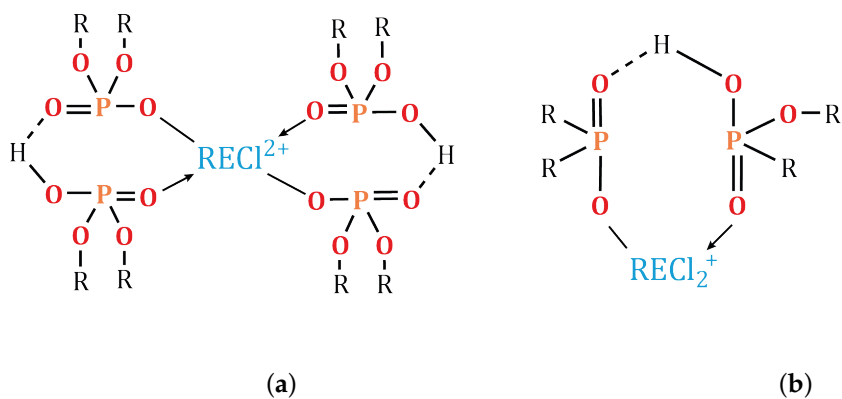


Figure 18. Structure of the extracted species. REH_2ClA_4 (a) and $REHCIBC$ (b).

3.5.3. Effect of O/A Ratio

The ratio of the organic phase to the aqueous phase (O/A) in the solvent extraction process plays an important role in the metal extraction process. Therefore, in this work, a series of experiments were carried out to determine the effect of the O/A ratio on the extraction of *La*, *Ce*, and *Nd* from a leaching liquor in a chloride medium that presented 2477.0 mg/L of *La*, 3512.5 mg/L of *Ce* and 2475.4 mg/L of *Nd*, using *D2EHPA* and *Cyanex 572*, both at 10% in n-heptane as organic extraction phases. When using *D2EHPA* the *La* extraction increases from 6.1% to 76.7%, *Ce* extraction increases from 14.1% to 90.6% and *Nd* extraction increases from 26.7% to 95.5% with the increase of O/A ratio from 1:2 to 5:1 (Figure 19a). In the case of *Cyanex 572* the increase of O/A ratio from 1:2 to 5:1 implies the increase in the extraction of *Ce* from 3.7% to 37.1%; *La* from 1.6% to 27.3% and *Nd* from 4.4% to 68.4% (Figure 19b). In both cases, this behavior is due to the increase in the availability of reagents for extraction. In all experiments, the pH was kept at 0.5 and the contact time at 30 min.

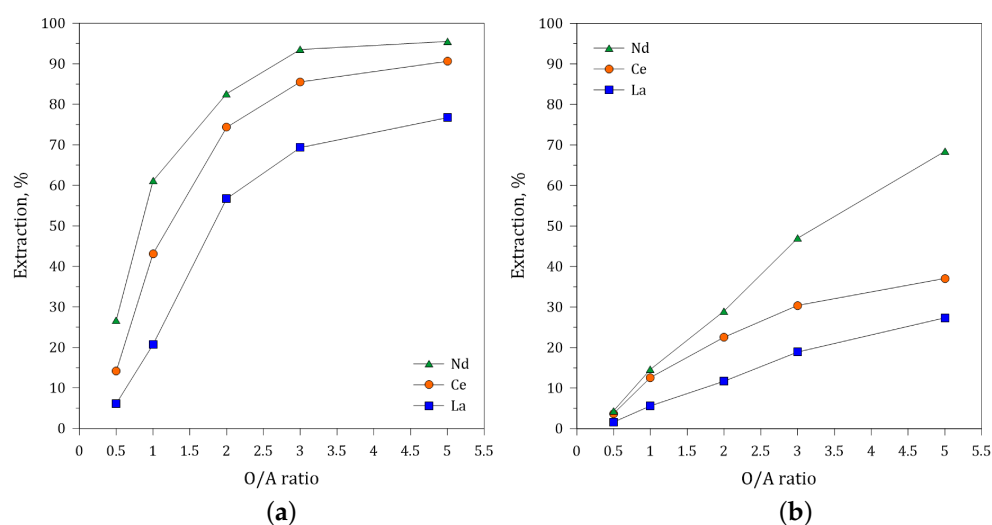


Figure 19. Effect of the O/A ratio on the extraction of *Ce*, *La* and *Nd* with: *D2EHPA* (a) and *Cyanex 572* (b).

Considering that the extraction efficiency is higher with *D2EHPA*, the number of theoretical stages required in countercurrent for the complete recovery of *La*, *Ce*, and *Nd* from the leach liquor was determined; for this, McCabe–Thiele diagrams were constructed with *D2EHPA* at 10% in n-heptane. In these experiments, the volume ratio of the organic to aqueous phase varied from 2:1 to 5:1. The McCabe–Thiele diagrams for the extraction of *Ce*, *La*, and *Nd* are shown in Figure 20. Three theoretical extraction steps are required to extract *Ce* at an O/A ratio of four quantitatively. For the extraction of *La*, three extraction steps are required with an O/A ratio of eight and for the extraction of *Nd*, three extraction steps with an O/A ratio of two are required. The experimental data for the determination of the extraction efficiencies with the change of the O/A ratio and the construction of the McCabe–Thiele diagrams can be seen in Table 5.

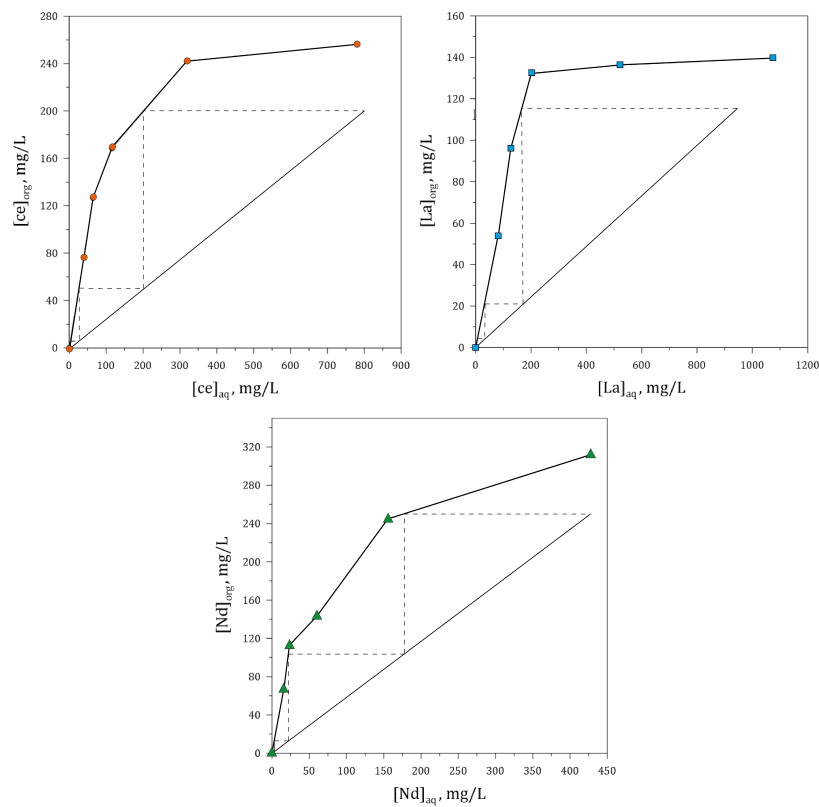


Figure 20. McCabe–Thiele diagrams for the extraction of *Ce*, *La*, and *Nd* with D2EHPA at 10% *v/v* in n-heptane.

Table 5. Experimental data for the calculation of the extraction efficiency of *Ce*, *La*, and *Nd* with the change of the O/A ratio.

O/A Ratio	0.5	1	2	3	5
V_{aq} , (mL)	360	300	180	150	100
V_{org} , (mL)	180	300	360	450	500
$[Ce]_i$, (mg/L)	1036.7	562.0	285.6	191.2	115.6
$[La]_i$, (mg/L)	1214.3	658.3	334.5	224.0	135.4
$[Nd]_i$, (mg/L)	740.0	401.1	203.9	136.5	82.5
<i>D2EHPA</i>					
$[Ce]_a$, (mg/L)	780.5	319.8	116.8	64.5	39.5
D_{Ce}	0.3	0.8	1.4	2.0	1.9
E_{Ce} , (%)	14.1	43.1	74.3	85.5	90.6
$[La]_a$, (mg/L)	1074.6	522.0	202.2	127.8	81.7
D_{La}	0.1	0.3	0.7	0.8	0.7
E_{La} , (%)	6.1	20.7	56.7	69.3	76.7
$[Nd]_a$, (mg/L)	428.1	156.0	60.4	23.6	15.7
D_{Nd}	0.7	1.6	2.4	4.8	4.2
E_{Nd} , (%)	26.7	61.1	82.6	93.5	95.5
<i>Cyanex 572</i>					
$[Ce]_a$, (mg/L)	962.8	491.2	249.3	166.4	103.4
D_{Ce}	0.08	0.14	0.15	0.15	0.12
E_{Ce} , (%)	3.7	12.6	22.5	30.4	37.1
$[La]_a$, (mg/L)	1176.0	321.4	313.8	207.9	126.0
D_{La}	0.03	0.06	0.07	0.08	0.08
E_{La} , (%)	1.6	5.6	11.7	18.9	27.3
$[Nd]_a$, (mg/L)	677.6	342.6	169.3	105.4	57.6
D_{Nd}	0.09	0.17	0.20	0.30	0.43
E_{Nd} , (%)	4.4	14.6	29.0	47.0	68.4

3.5.4. Separation Factor (SF)

The complex-forming nature of metal ions affects their relative affinity to the extractant agents and results in a marked difference in the extraction capacity that enables metal separation [51]. The role of the separation factor (SF) is important in comparing the separation ability of the RE; the separation factor must always be greater than one for the

RE to achieve effective separation [20]. The separation between two metals is not possible if their separation factor is equal to or less than unity [24]; RE has very similar chemical properties and is quite difficult to separate from each other. In the present investigation, the *Ce/La*, *Nd/La*, and *Nd/Ce* separation factor was determined with *D2EHPA* and *Cyanex 572* at different pH; it was found that the SF value changes with the change of solution pH, for both extracting agents (Table 6). In the case of extraction with *D2EHPA*, the separation factor for *Ce/La* was 3.04 at pH 0.5, for *Nd/La* it was 2.32 at pH 0.2, and for *Nd/Ce* it was 6.4 at pH 0.5. In the case of separation with *Cyanex 572*, the highest separation factor for *Ce/La* was 5.3, which was achieved at pH 0.2, while for *Nd/Ce* and *Nd/La*, the separation factors were 2.1 and 7.9, respectively and were achieved at pH 2.0. Critical observation of the results indicates that there is a low and rare separation factor.

Table 6. Separation factors of *Ce*, *La* and *Nd* with *D2EHPA* and *Cyanex 572*.

pH	Separation Factor					
	<i>Ce/La</i>		<i>Nd/Ce</i>		<i>Nd/La</i>	
	<i>D2EHPA</i>	<i>Cy 572</i>	<i>D2EHPA</i>	<i>Cy 572</i>	<i>D2EHPA</i>	<i>Cy 572</i>
0.2	1.34	5.30	2.32	0.54	3.11	2.86
0.5	3.04	2.43	2.11	1.19	6.42	2.88
1.0	2.42	2.22	1.61	1.12	3.90	2.49
1.5	2.89	2.58	1.88	1.44	5.42	3.72
2.0	1.00	3.83	1.50	2.05	1.50	7.86
2.5	1.28	3.87	1.48	2.00	1.89	7.73

4. Conclusions

In this study, a residue from alluvial gold mining has been considered, which has monazite in its composition; therefore, a systematic analysis was carried out for the recovery of *La*, *Ce*, and *Nd* present in this monazite. The dephosphorization process of the monazite concentrate succeeded in removing approximately 86% of phosphate with *KOH* as a baking reagent. The *HCl* leaching study achieved leaching yields of 62.2% *Ce*, 95.8% *La*, and 94.3% *Nd*. An extraction yield of 100% of *La*, *Ce*, and *Nd* was obtained with *D2EHPA* at a 1:1 (O/A) ratio. Using the McCabe–Thiele diagrams, it was possible to determine the requirement of three extraction stages with *D2EHPA* to maximize the recovery of *Ce*, *La*, and *Nd* with O/A ratios of 4, 8, and 2, respectively.

Author Contributions: Conceptualization/methodology/investigation/writing—original draft preparation, L.E.-V.; Conceptualization/writing—review and editing/supervision/project administration/funding acquisition, L.M.O.-C. All authors have read and agreed to the published version of the manuscript.

Funding: This research was funded by MINCIENCIAS/110180863804.

Acknowledgments: The authors wish to thank the Colombian Ministry of Science (MINCIENCIAS) for the financial support granted to the project “Recovery of rare earth elements from minerals present in black sands, residue from alluvial gold mining in El Bagre-Antioquia”, code 110180863804 within Call for Projects 808 of 2018-CFP for Science, Technology and Innovation projects and their contribution to the country’s challenges. The authors would also like to thank the company Mineros Aluvial S.A.S BIC for the donation of the residual sands from alluvial gold mining.

Conflicts of Interest: The authors declare no conflict of interest.

References

- Rybak, J.; Gorbatyuk, S.M.; Kongar-Syuryun, C.; Khayrutdinov, A.M.; Tyulyaeva, Y.; Makarov, P.S. Utilization of Mineral Waste: A Method for Expanding the Mineral Resource Base of a Mining and Smelting Company. *Metallurgist* **2021**, *64*, 851–861. [CrossRef]
- Lucas, J.; Lucas, P.; Mercier, T.L.; Rollat, A.; Davenport, W. *Rare Earths Science, Technology, Production and Use*, 1st ed.; Elsevier: Amsterdam, The Netherlands, 2015.
- Suli, L.M.; Ibrahim, W.H.W.; Aziz, B.A.; Deraman, M.R.; Ismail, N.A. A Review of Rare Earth Mineral Processing Technology. *Chem. Eng. Res. Bull* **2017**, *19*, 20–35. [CrossRef]
- Zglinicki, K.; Malek, R.; Szamalek, K.; Wolkowicz, S. Mining Waste as a Potential Additional Source of HREE and U for the European Green Deal: A Case Study of Bangka Island (Indonesia). *Minerals* **2022**, *12*, 44. [CrossRef]
- Kim, K.; Jeong, S. Separation of monazite from placer deposit by magnetic separation. *Minerals* **2019**, *9*, 149. [CrossRef]

6. Abaka-Wood, G.B.; Addai-Mensah, J.; Skinner, W. The Use of Mining Tailings as Analog of Rare Earth Elements Resources: Part 1—Characterization and Preliminary Separation. *Miner. Process. Extr. Metall. Rev.* **2021**, *43*, 701–715. [[CrossRef](#)]
7. Yang, Y.; Walton, A.; Sheridan, R.; Guth, K.; Gaub, R.; Gutfleich, O.; Buchert, M.; Steenari, B.; Gerven, T.M.; Jones, P.T.; et al. REE Recovery from End-of-Life NdFeB Permanent Magnet Scrap: A Critical Review. *J. Sustain. Metall.* **2017**, *3*, 122–149. [[CrossRef](#)]
8. Abaka-Wood, G.B.; Zanin, M.; Addai-Mensah, J.; Skinner, W. Recovery of rare earth elements minerals from iron oxide–silicate rich tailings—Part 1: Magnetic separation. *Miner. Eng.* **2019**, *136*, 50–61. [[CrossRef](#)]
9. Lamus-Molina, A. *Minerología Aplicada al uso y Aprovechamiento de las Arenas Negras (El Bagre, Antioquia)*; Universidad Nacional de Colombia: Medellín, Colombia, 2005.
10. Kerguelen, J. *Caracterización y Aprovechamiento de Recursos Minerales en Colas de Terrazas Aluviales del Distrito Bagre-Nechí*; Universidad Nacional de Colombia: Medellín, Colombia, 2016.
11. Udayakumar, S.; Mohd-Noor, A.F.; Abdul-Hamid, S.A.; Rama-Putra, T.A.; Anderson, C.G. Chemical and Mineralogical Characterization of Malaysian Monazite Concentrate. *Mining, Metall. Explor.* **2020**, *37*, 415–431. [[CrossRef](#)]
12. Amer, T.A.; El-Sheikh, E.M.; Hassanin, M.A.; Fathy, W.M. Processing of Monazite Mineral Concentrate for Selective Recovery of Uranium. *Chem. Afr.* **2019**, *2*, 123–134. [[CrossRef](#)]
13. Tunsu, C.; Menard, Y.; Eriksen, D.Ø.; Erberg, C.; Petranicova, M. Recovery of critical materials from mine tailings: A comparative study of the solvent extraction of rare earths using acidic, solvating and mixed extractant systems. *J. Clean. Prod.* **2019**, *218*, 425–437. [[CrossRef](#)]
14. Zglinicki, K.; Szamałek, K.; Szamalek, K.; Wolkowicz, S. Critical Minerals from Post-Processing Tailing. A Case Study from Bangka Island, Indonesia. *Minerals* **2021**, *11*, 352. [[CrossRef](#)]
15. Dehaine, Q.; Filippov, L.O.; Joussemet, R. Rare earths (La, Ce, Nd) and rare metals (Sn, Nb, W) as by-products of kaolin production—Part 2: Gravity processing of micaceous residues. *Miner. Eng.* **2017**, *100*, 200–210. [[CrossRef](#)]
16. Norgate, T.; Jahanshahi, S. Low grade ores - Smelt, leach or concentrate? *Miner. Eng.* **2010**, *23*, 65–73. [[CrossRef](#)]
17. Berry, L.; Agarwal, V.; Galvin, J.; Safarzadeh, M.S. Decomposition of monazite concentrate in sulphuric acid. *Can. Metall. Q.* **2018**, *57*, 422–433. [[CrossRef](#)]
18. Udayakumar, S.; Rezan, S.A.; Noor, A.F.M.; Putra, T.A.R.; Ibrahim, I.; Baharun, N. The dephosphorization behaviour of Malaysian monazite concentrates. In AIP Conference Proceedings, Penang, Malaysia, 31 October–1 November 2019
19. Ni, Y.; Hughes, J.M.; Mariano, A.N. Crystal chemistry of the monazite and xenotime structures. *Am. Miner.* **1995**, *80*, 21–26. [[CrossRef](#)]
20. Kumari, A.; Jha, M.K.; Yoo, K.; Panda, R.; Lee, J.Y.; Kumar, J.R.; Pathak, D.D. Advanced process to dephosphorize monazite for effective leaching of rare earth metals (REMs). *Hydrometallurgy* **2019**, *187*, 203–211. [[CrossRef](#)]
21. Clavier, N.; Podor, R.; Dacheux, N. Crystal chemistry of the monazite structure. *J. Eur. Ceram. Soc.* **2011**, *31*, 941–976. [[CrossRef](#)]
22. Kumari, A.; Panda, R.; Jha, M.K.; Kumar, J.R.; Lee, J.Y. Process development to recover rare earth metals from monazite mineral: A review. *Miner. Eng.* **2015**, *79*, 102–115. [[CrossRef](#)]
23. Jordens, A.; Cheng, Y.P.; Waters, K.E. A review of the beneficiation of rare earth element bearing minerals. *Miner. Eng.* **2013**, *41*, 97–114. [[CrossRef](#)]
24. Kumari, A.; Panda, R.; Lee, J.Y.; Thriveni, T.; Jha, M.K.; Pathak, D.D. Extraction of rare earth metals (REMs) from chloride medium by organo-metallic complexation using D2EHPA. *Sep. Purif. Technol.* **2019**, *227*, 115680. [[CrossRef](#)]
25. Krishnamurthy, N.; Gupta, G.K. *Extractive Metallurgy of Rare Earths*, 2nd ed.; CRC Press: Boca Raton, FL, USA, 2016.
26. Peelman, S.; Zhi, H.I.S.; Jilt, S.; Yang, Y. Leaching of Rare Earth Elements: Review of Past and Present Technologies In *Rare Earths Industry Technological, Economic, and Environmental Implications*; De Lima, L., Filho, W., Eds.; Elsevier: Amsterdam, The Netherlands, 2016; pp. 319–334.
27. Walawalkar, M.; Nichol, C.K.; Azimi, G. Process investigation of the acid leaching of rare earth elements from phosphogypsum using HCl, HNO₃, and H₂SO₄. *Hydrometallurgy* **2016**, *166*, 195–204. [[CrossRef](#)]
28. Jorjani, E.; Shahbazi, M. The production of rare earth elements group via tributyl phosphate extraction and precipitation stripping using oxalic acid. *Arab. J. Chem.* **2016**, *9*, S1532–S1539. [[CrossRef](#)]
29. Flett, D.S. Solvent extraction in hydrometallurgy: The role of organophosphorus extractants. *J. Organomet. Chem.* **2005**, *690*, 2426–2438. [[CrossRef](#)]
30. Gupta, B.; Malik, P.; Deep, A. Solvent extraction and separation of trivalent Lanthanides and Yttrium using Cyanex 923. *Solvent Extr. Ion Exch.* **2003**, *21*, 239–258. [[CrossRef](#)]
31. Hefiny, N.E.; Daoud, J.A. Extraction and separation of thorium(IV) and praseodymium (III) with CYANEX 301 and CYANEX 302 from nitrate medium. *J. Radioanal. Nucl. Chem.* **2004**, *261*, 357–363. [[CrossRef](#)]
32. Sun, X.; Zhao, J.; Meng, S.; Li, D. Synergistic extraction and separation of yttrium from heavy rare earths using mixture of sec-octylphenoxy acetic acid and bis(2,4,4-trimethylpentyl) phosphinic acid. *Anal. Chim. Acta* **2005**, *533*, 83–88. [[CrossRef](#)]
33. Miranda, T.; Zinner, B. Separation of samarium and gadolinium solutions by solvent extraction. *J. Alloys Compd.* **1997**, *249*, 116–118. [[CrossRef](#)]
34. Correa, M.M.J.; Silvas, F.P.C.; Alipradini, P.; Moraes, V.T.; Dreisinger, D.; Espinosa, D.C.R. Separation of copper from a leaching solution of printed circuit boards by using solvent extraction with D2EHPA. *Braz. J. Chem. Eng.* **2018**, *35*, 919–930. [[CrossRef](#)]
35. Wang, Y.; Li, F.; Zhao, Z.; Dong, Y.; Sun, X. The novel extraction process based on CYANEX[®] 572 for separating heavy rare earths from ion-adsorbed deposit. *Sep. Purif. Technol.* **2015**, *151*, 303–308. [[CrossRef](#)]

36. Wang, J.; Xu, S.; Li, L.; Li, J. Synthesis of organic phosphinic acids and studies on the relationship between their structure and extraction-separation performance of heavy rare earths from HNO_3 solutions. *Hydrometallurgy* **2013**, *137*, 108–114. [[CrossRef](#)]
37. Huang, X.; Li, J.; Long, Z.; Zhang, Y.; Xue, X.; Zhu, Z. Synergistic extraction of rare earth by mixtures of 2-ethylhexyl phosphoric acid mono-2-ethylhexyl ester and di-(2-ethylhexyl) phosphoric acid from sulfuric acid medium. *J. Rare Earths* **2008**, *26*, 410–413. [[CrossRef](#)]
38. Thakur, N.V. Separation of rare earths by solvent extraction. *Miner. Process. Extr. Metall. Rev.* **2000**, *21*, 277–306. [[CrossRef](#)]
39. Moustafa, M.I.; Abdelfattah, N.A. Physical and chemical beneficiation of the egyptian beach monazite. *Resour. Geol.* **2010**, *60*, 288–299. [[CrossRef](#)]
40. Panda, R.; Kumari, A.; Jha, M.K.; Hait, J.; Kumar, V.; Kumar, J.R.; Lee, J.Y. Leaching of rare earth metals (REMs) from Korean monazite concentrate. *J. Ind. Eng. Chem.* **2014**, *20*, 2035–2042. [[CrossRef](#)]
41. Trinh, H.B.; Lee, J.C.; Srivastava, R.R.; Kim, S.; Ilyas, S. Eco-threat Minimization in HCl Leaching of PGMs from Spent Automobile Catalysts by Formic Acid Prereduction. *ACS Sustain. Chem. Eng.* **2017**, *5*, 7302–7309. [[CrossRef](#)]
42. Innocenzi, V.; Ippolito, N.M.; Pietrelli, L.; Centofanti, M.; Piga, L.; Vegliò, F. Application of solvent extraction operation to recover rare earths from fluorescent lamps. *J. Clean. Prod.* **2018**, *172*, 2840–2852. [[CrossRef](#)]
43. Abaka-Wood, G.B.; Addai-Mensah, J.; Skinner, W. Review of Flotation and Physical Separation of Rare Earth Element Minerals. In Proceedings of the 4th UMaT Biennial International Mining and Mineral Conference, Tarkwah, Ghana, 3–6 August 2016.
44. Kelly, E.G.; Spottiswood, D.J. *Introduction to Mineral Processing*, 1st ed.; John Wiley & Sons: Hoboken, NJ, USA, 1990.
45. Abo-Atia, T.; Wouters, W.; Monforte, G.; Spooen, J. Microwave chloride leaching of valuable elements from spent automotive catalysts: Understanding the role of hydrogen peroxide. *Resour. Conserv. Recycl.* **2021**, *166*, 105349. [[CrossRef](#)]
46. Xu, Y.; Liu, H.; Meng, Z.; Cui, J.; Zhao, W.; Li, L. Decomposition of bastnasite and monazite mixed rare earth minerals calcined by alkali liquid. *J. Rare Earths* **2012**, *30*, 155–158. [[CrossRef](#)]
47. Chi, R.; Li, Z.; Peng, C.; Gao, H.; Xu, Z. Preparation of enriched cerium oxide from bastnasite with hydrochloric acid by two-step leaching. *Metall. Mater. Trans. B* **2006**, *37*, 155–160. [[CrossRef](#)]
48. Zhang, C.; Wang, L.; Huang, X.; Dong, J.; Long, Z.; Zhang, Y. Yttrium extraction from chloride solution with a synergistic system of 2-ethylhexyl phosphonic acid mono-(2-ethylhexyl) ester and bis(2,4,4- trimethylpentyl) phosphinic acid. *Hydrometallurgy* **2014**, *147–148*, 7–12. [[CrossRef](#)]
49. Liu, Y.; Jeon, H.S.; Lee, M. Solvent extraction of Pr and Nd from chloride solutions using ternary extractant system of Cyanex 272, Alamine 336 and TBP. *J. Ind. Eng. Chem.* **2015**, *31*, 74–79. [[CrossRef](#)]
50. Acharya, S.; Mishra, S.; Misra, P.K. Studies on extraction and separation of La(III) with DEHPA and PC88A in petrofin. *Hydrometallurgy* **2015**, *156*, 12–16. [[CrossRef](#)]
51. Kim, J.S.; Nagaphani-Kumar, B.; Lee, J.Y.; Lakshmi-Kantam, M.; Ramachandra-Reddy, B. Separation and Recovery of Light Rare-Earths from Chloride Solutions using Organophosphorus based Extractants. *Sep. Sci. Technol.* **2012**, *47*, 1644–1650. [[CrossRef](#)]